

Faraday Discussions

Accepted Manuscript



This is an Accepted Manuscript, which has been through the Royal Society of Chemistry peer review process and has been accepted for publication.

Accepted Manuscripts are published online shortly after acceptance, before technical editing, formatting and proof reading. Using this free service, authors can make their results available to the community, in citable form, before we publish the edited article. We will replace this Accepted Manuscript with the edited and formatted Advance Article as soon as it is available.

You can find more information about Accepted Manuscripts in the [Information for Authors](#).

Please note that technical editing may introduce minor changes to the text and/or graphics, which may alter content. The journal's standard [Terms & Conditions](#) and the [Ethical guidelines](#) still apply. In no event shall the Royal Society of Chemistry be held responsible for any errors or omissions in this Accepted Manuscript or any consequences arising from the use of any information it contains.

This article can be cited before page numbers have been issued, to do this please use: L. Walters, A. R. Neale, T. Samarakoon, K. Chae, R. J. Nichols and L. J. Hardwick, *Faraday Discuss.*, 2026, DOI: 10.1039/D5FD00174A.

***In situ* ATR-SEIRAS investigations on the effects of Li⁺ and dissolved O₂ on
electrochemical interfacial reorganisation in an ionic liquid**

View Article Online

DOI: 10.1039/D5FD00174A

Lucy J. Walters^a, Alex R. Neale^{*a}, Thukshan Samarakoon^a, Kyunghee Chae^{a,b}, Richard Nichols^c, Laurence J. Hardwick^{a*}

^aStephenson Institute for Renewable Energy, Department of Chemistry, University of Liverpool, Liverpool, L69 7ZF, UK

^bDepartment of Chemistry and Nano Science, Division of Molecular and Life Sciences, College of Natural Sciences, Ewha Womans University, 52, Ewhayeodae-gil, Seodaemun-gu, Seoul, 03760, Republic of Korea

^cDepartment of Chemistry, University of Liverpool, Liverpool, L69 7ZD, UK

*Corresponding authors: alex.neale@liverpool.ac.uk; hardwick@liverpool.ac.uk



Abstract

View Article Online
DOI: 10.1039/D5FD00174A

Interfacial reorganisation at a gold electrode within an ionic liquid (1-methyl-1-propylpyrrolidinium bis{(trifluoromethyl)sulfonyl}imide, ([Pyrr₁₃][TFSI])) electrolyte was investigated *via in situ* electrochemical attenuated total reflection surface-enhanced infrared absorption spectroscopy (ATR-SEIRAS). The *in situ* cell incorporated a micromachined Si wafer internal reflection element, that enabled the spectral recording down to 500 cm⁻¹. Cation-anion restructuring of the double layer in the aprotic ionic liquid, [Pyrr₁₃][TFSI], was explored under varying potential windows within the extended wavenumber range of 4000-500 cm⁻¹. Double layer restructuring was found to be significantly impeded by inclusion of low concentrations of Li-salt (0.001 M Li[TFSI]). The presence of Li⁺ led to the formation of [Li[TFSI]_x]^(x-1) complexes and aggregates which disrupt the periodicity of the double layer of the neat ionic liquid. The inclusion of dissolved O₂ into [Pyrr₁₃][TFSI] led to irreversible promotion of double layer rearrangement with the redox active solute with coordinating properties with cation (O₂⁻ ---[Pyrr₁₃]⁺).



Introduction

View Article Online
DOI: 10.1039/D5FD00174A

Ionic liquids (ILs) represent unique, non-classical type of electrolyte due to the lack of solvating molecular solvents and being purely ionic in character. As such, in response to the electric field at the electrode surface, the accumulation of charge does not follow conventional double layer models, where the potentials decay at increasing distance from the electrode surface according to Helmholtz planes and diffuse layers that are observed with solvated ions in solution in molecular solvents. Instead, the charge distribution outward from the surface is more periodical, showing an organisation of alternating ions and counter-ions. Room temperature ionic liquids (RTILs) are candidate battery electrolytes, particularly for open cell systems, such as metal-air, due to their wide electrochemical windows, negligible volatility, high chemical stability and non-flammability.¹⁻⁶ The varying arrangement and structure of the ILs at the electrochemical interface under potential control is of particular research interest to enable the design of RTIL/electrode interfaces that are optimised for a particular electrochemical reaction.

Vibrational and nonlinear spectroscopic techniques, such as surface-enhanced infrared absorption spectroscopy (SEIRAS), infrared reflection absorption, surface enhanced Raman, and sum frequency generation spectroscopies, are particularly useful for gaining insight into dynamic processes that occur at the RTIL/electrode interface, due to the high level of surface selectivity and sensitivity, and the ability to couple with varying electrochemical procedures.⁷⁻

15

Pyrrolidinium-based ILs have been shown to deliver stable cycling performance within metal-O₂ cells.^{16, 17} 1-methyl-1-propylpyrrolidinium bis{(trifluoromethyl)sulfonyl}imide ([Pyrr13][TFSI]) in particular has been previously investigated using *in situ* electrochemical attenuated total reflection (ATR-SEIRAS) and found that an asymmetric hysteresis of ion



replacement at the surface occurred.¹⁸ Cation-to-anion replacement takes place around the potential of zero charge (pzc), but a significant overpotential was necessary for anion-to-cation replacement. This contrasted to an earlier study on an imidazolium based RTIL, which displayed a symmetric hysteresis.¹⁵ The difference in behaviour between the imidazolium and pyrrolidinium-based ILs was explained by the difference in polarisability of the two cations. In the pyrrolidinium-based cation, the charge is considerably more localised, whereas the aromatic character of imidazolium cation allows the charge distribution around the molecule to change significantly when a potential is applied. The change in spatial distribution of charge results in improved screening ability of the imidazolium cation, and therefore weaker short-range ion interactions. For anion-to-cation replacement, the polarisation of [TFSI]⁻ at the interface is compensated for by the highly polarisable imidazolium-based cation. With the pyrrolidinium-based cation, the polarisation of [TFSI]⁻ at the interface cannot be effectively screened by the localised charge on the cation, so the short-range ordering is more stable and an overpotential is required for ion replacement.

Many infrared (IR) peaks of interest occur below 1000 cm⁻¹, however within *in situ* electrochemical IR studies the typical Si prisms used as internal reflection elements (IREs) have cut off at or above 1000 cm⁻¹. A few different approaches to mitigate the Si cut-off have been reported; for IREs in ATR-IR spectroscopy using thin, micromachined or cleaved Si wafers,¹⁹⁻²² or by sandwiching Si wafers to support materials with better low frequency throughput, such as ZnSe.^{23, 24} However, the arrangement of multilayer IREs introduced reflection losses due to the interfaces between the materials of differing refractive indices. Furthermore, achieving uniform contact between the materials presented a challenge. Schumacher *et al.* reported the fabrication of microgroove Si wafers by anisotropic wet etching, which were then used in ATR-IR experiments analysing organic and inorganic species.²⁵ Microgroove Si IREs were commercialised by IRUBIS GmbH in 2017 and, in the same year,



Morhart *et al.* reported use of the IREs for electrochemical ATR-SEIRAS.²⁶ Therein, employing a thin (*ca.* 20 nm) Au film deposited on the flat surface of the Si wafer, the authors demonstrated the extension of the SEIRAS measurement range with the Si wafers down to 500 cm⁻¹ in an aqueous system, with the potential for further extension below 500 cm⁻¹ with a detector capable of measuring into the far-IR range. The authors showed that the wafers can generate ATR-SEIRA spectra comparable to spectra generated using Si hemispheres above 1500 cm⁻¹ and, critically, outperforming the hemispheres at frequencies lower than 1500 cm⁻¹. Herein, the reordering of [Pyrr₁₃][TFSI] at a Au/IL interface is investigated using ATR-SEIRAS at a thin microgroove Si wafer IRE within an extended wavenumber range from 4000 down to 500 cm⁻¹. The effect on the interface structure within an IL is investigated under potential control in the presence of Li⁺ and dissolved O₂ to understand the structure of interfaces with Li-O₂ relevant IL-based electrolytes.

View Article Online

DOI: 10.1039/D5FD00174A



Experimental

View Article Online

DOI: 10.1039/D5FD00174A

Atomic force microscopy (AFM) images were taken using tapping mode with a single crystal silicon CSG30 cantilever (force constant 0.6 N m^{-1} , resonant frequency 48 kHz). Scanning electron microscopy (SEM) images were taken using a Tescan S8000G scanning electron microscope with accelerating voltage 5 kV and beam current 1 nA. A Bruker Vertex 70v FTIR spectrometer equipped with a liquid nitrogen cooled MCT (mercury cadmium telluride) detector was used to record *in situ* SEIRA spectra in the range of $4000\text{-}500 \text{ cm}^{-1}$. Unpolarised radiation was used for all measurements. Spectra were collected every 30 seconds at 4 cm^{-1} resolution with a 6 mm aperture. The angle of incidence was set to 55° and was controlled using a PIKE VeeMAX III ATR accessory. Electrochemical measurements were performed using a Bio-Logic SP-50 potentiostat.

A micromachined Si wafer (IRUBIS GmbH) was used as the internal reflection element (IRE). The flat surface of the wafer was polished sequentially using Buehler MicroPolish alumina powder with grain sizes of 1, 0.3, and $0.05 \mu\text{m}$ respectively, then sonicated in a 50/50 mixture of ethanol and Milli-Q® water ($18.2 \text{ M}\Omega$) for *ca.* two minutes, sonicated in pure Milli-Q® water for *ca.* two minutes, then dried in a $70 \text{ }^\circ\text{C}$ oven. The Au layer (Au wire, Advent RM, 99.95%) was thermally evaporated on the polished side of the wafer in a two-step process, using a Leybold Univex 300 thermal evaporation system under vacuum at 10^{-6} Torr. Using a 3D printed mask, an 18 nm Au layer was first deposited on a small portion of the IRE. The mask was then removed, and a 20 nm Au layer was deposited on the entire IRE surface at a deposition rate of 0.1 \AA s^{-1} . This resulted in a thicker 38 nm region for electrical contact, and a thinner 20 nm SEIRAS active region. Comparative transmission measurements were conducted using a conventional Si prism IRE (60° face-angled prism, PIKE) following the same deposition regime for the Au layer as above.



The spectroelectrochemical cell (**Figure 1**) used for SEIRAS was custom designed and built using CNC (computer numeric control) machining in poly ether ether ketone (PEEK). Prior to measurements, all cell components were sonicated in ethanol and Milli-Q® water, and then further rinsed with Milli-Q® water. An Ag wire quasi-reference electrode was used, which was cleaned by removing surface impurities with a scalpel, followed by a cleaning step with ethanol and Milli-Q® water. A coiled Pt wire was used as the counter electrode, which was annealed with a propane/butane blowtorch until glowing orange, then washed with ethanol and Milli-Q® water. All cell components were dried overnight in a 70 °C oven before being transferred to the Ar-filled glovebox (< 0.1 ppm O₂, < 0.1 ppm H₂O) for cell preparation.

View Article Online

DOI: 10.1039/D5FD00174A

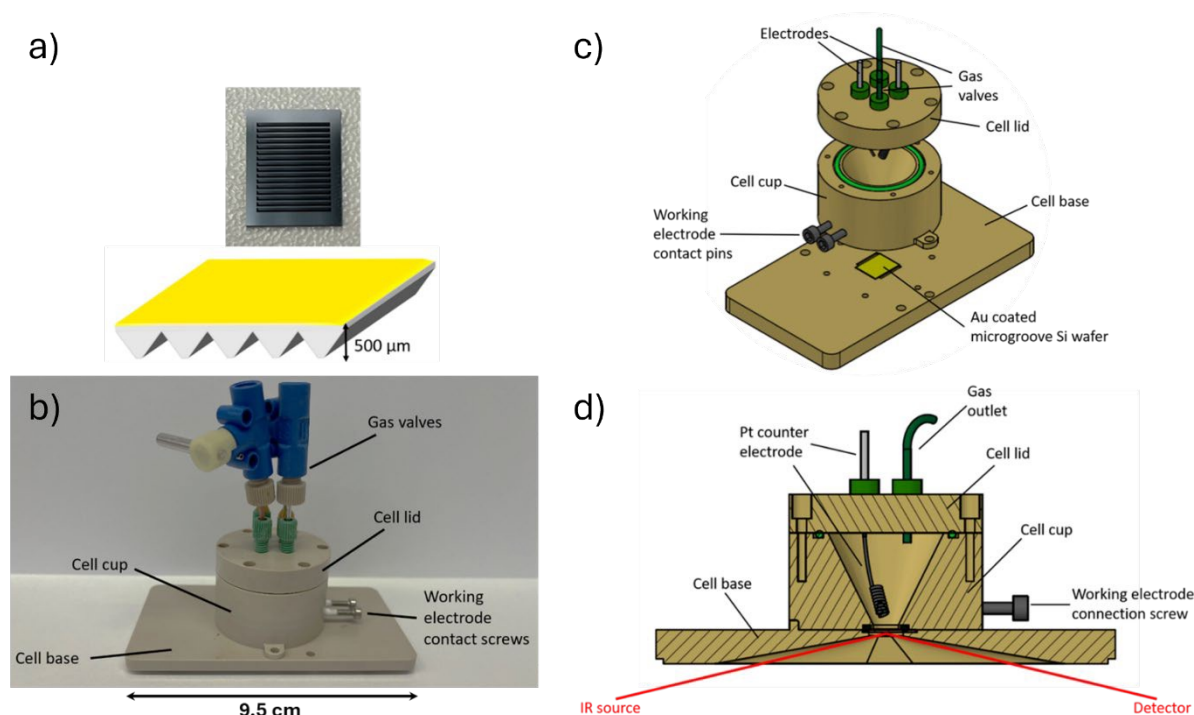


Figure 1. (a) Photograph (top) and schematic (bottom) of the Si microgroove wafer Internal Reflection Element used in this work. (b) Photograph of the sealed spectroelectrochemical cell and (c - d) schematics of the cell structure and internal configuration. Due to the position of the model cross section in (d), the Ag wire pseudo reference electrode is not shown.



The cell was then filled with electrolyte and sealed inside the Ar-filled glove box. All electrolyte materials were stored and handled inside the glovebox. The electrolytes used were neat 1-methyl-1-propylpyrrolidinium bis{(trifluoromethyl)sulfonyl}imide ([Pyrr₁₃][TFSI], **Figure 2**) (99.9%, < 20 ppm H₂O, Solvionic) and 1 mM and 100 mM solutions of Li[TFSI] (99.5%, < 20 ppm H₂O, Solvionic) prepared gravimetrically with [Pyrr₁₃][TFSI] as the solvent. For experiments in an oxygen atmosphere, the cell was purged with O₂ (BOC, 99.9995% purity) for a minimum of 30 mins and sealed using the attached valves. The Au working electrode had an active area diameter of 0.6 cm, with an area of 0.283 cm². A typical electrolyte volume of 500 μL led to a cell flooding factor (electrolyte volume per electrode area) of around 1800 μL cm⁻².

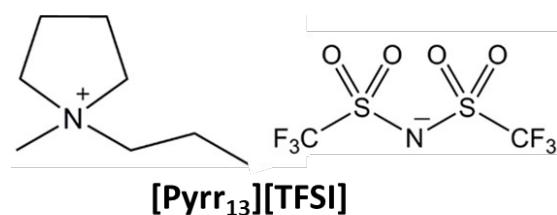


Figure 2. Chemical structure of the IL 1-methyl-1-propylpyrrolidinium bis{(trifluoromethyl)sulfonyl}imide ([Pyrr₁₃][TFSI]) used in this work.

Spectra were collected at a defined reference potential (described below), then the potential was varied by cyclic voltammetry at 2 mV s⁻¹, with spectra continuously collected during the potential sweeps. Following spectroelectrochemical measurements, a small amount of ferrocene (Fc, Sigma) was added to the cell (handled inside the Ar glovebox) and the Fc⁺/Fc redox couple was used as an internal reference to compare cell voltages using the Ag quasi-reference electrode.

Information from SEIRAS measurements is presented in the form of difference spectra, giving information on relative changes at the surface as a function of the electrochemistry occurring



at the interface. In these spectra, positive-going peaks indicate an increase of a species close at the surface, and negative-going peaks indicate a loss of a species at the surface. To track the relative changes at the interface compared to the reference point, difference spectra were calculated according to the following formula:

$$\frac{\Delta S}{S} = \frac{S_{reference} - S_{variable}}{S_{reference}} \quad \text{Eq. 1}$$

Where S is a single channel spectrum, $S_{reference}$ is the single channel spectrum at the chosen reference potential, and $S_{variable}$ is the single channel spectrum at variable potentials. Peak integrations were carried out using the integration tool in Origin 2021b.

Cyclic voltammetry of the neat [Pyrr₁₃][TFSI] electrolyte at a conventional (non-thermally evaporated) Au working electrode (3 mm diameter, ALS) were performed in a custom glass cell sealed hermetically under Ar. The counter electrode was a Pt wire coil and the reference electrode was a silver wire immersed in a 0.1 M solution of silver trifluoromethanesulfonate (Ag[OTf]) in 1-butyl-1-methylpyrrolidinium [TFSI] ([Pyrr₁₄][TFSI]) within a glass capillary.²⁷ The Ag wire and Ag[OTf]/[Pyrr₁₄][TFSI] solution was isolated from the analyte electrolyte by a porous glass frit. The Au working electrode was polished using alumina slurries of decreasing particle size (1.0, 0.3, and 0.05 μm) in Milli-Q® water on microfibre cloth (Buehler). Between each polishing step, the electrode was rinsed and sonicated in a mixture of Milli-Q® H₂O and ethanol (1:1) for 2 mins to remove alumina particles, and additionally in Milli-Q® H₂O after the last step. The Pt wire coil was initially rinsed with ethanol and then Milli-Q® water and then flame annealed. Cell components were then dried above 80°C before being transferred to the Ar filled glovebox for cell sealing. After initial CV experiments, a small amount of ferrocene was added to the electrolyte to use the Fc⁺/Fc couple as an internal reference.

Raman spectra of bulk IL and IL/Li-salt solutions were collected using a Renishaw In-Via spectrometer coupled with a Leica inverted microscope with a 50x objective. Liquid



samples/solutions were sealed in glass vials and Raman spectra were collected using 785 nm laser excitation. The conventional ATR-FTIR spectrum (*i.e.*, no Au layer) was collected using a diamond-ATR accessory on a ThermoScientific Nicolet iS50 FTIR spectrometer housed inside a dry N₂ filled glovebox (H₂O and O₂ <0.1 ppm).

[View Article Online](#)

DOI: 10.1039/D5FD00174A



Au electrode and Si IRE characterisation

AFM and SEM images of the thermally evaporated Au film (**Figure 3**) to be used as the working electrode within the SEIRAS cell show a 10 nm thick discontinuous film with grain sizes of 30 - 40 nm within the percolating network. The morphology of the Au films resembles those reported previously that have delivered SEIRAS enhancement.^{28, 29}

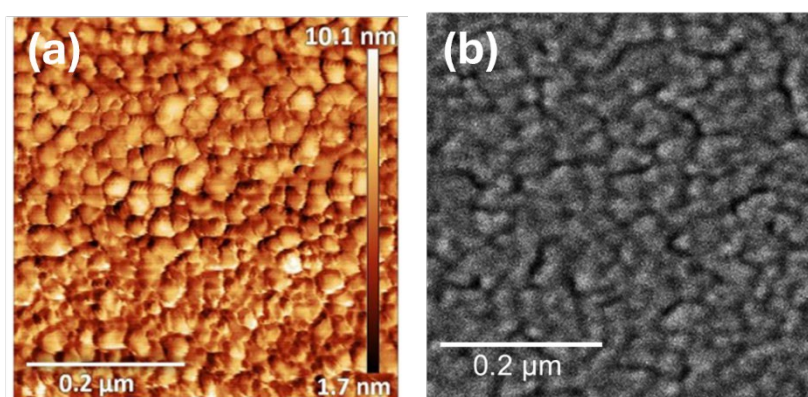


Figure 3. (a) Atomic force microscopy and (b) scanning electron microscopy images of a 20 nm thickness Au film deposited on Si wafer by thermal evaporation at 0.1 \AA s^{-1} , highlighting the nanostructured percolated network of the Au deposit.

The normalised infrared transmission through the Si microgroove wafer and Si prism IREs in the assembled SEIRAS cell, both comprising the 20 nm Au layer and neat [Pyrr₁₃][TFSI] electrolyte are compared in **Figure 4**. Where the transmission in the thicker Si prism drops to negligible levels below *ca.* 1000 cm^{-1} , crucially the transmission through the thin microgroove wafer remains significant down to below 500 cm^{-1} (beyond which a different detector would be required). This is in good agreement with previous observations.²⁶ While the overall absolute transmission is much lower with the wafer, below 1000 cm^{-1} this observation reverses and there is considerably greater IR transmission through the Si wafer than the prism.



Ultimately, this feature of the thin microgroove wafer overcomes the limitations of Si prism IREs and enables band detection in the 1000-500 cm^{-1} region, on a more electrochemically inert window, compared to ZnSe for example.

View Article Online
DOI: 10.1039/D5FD00174A

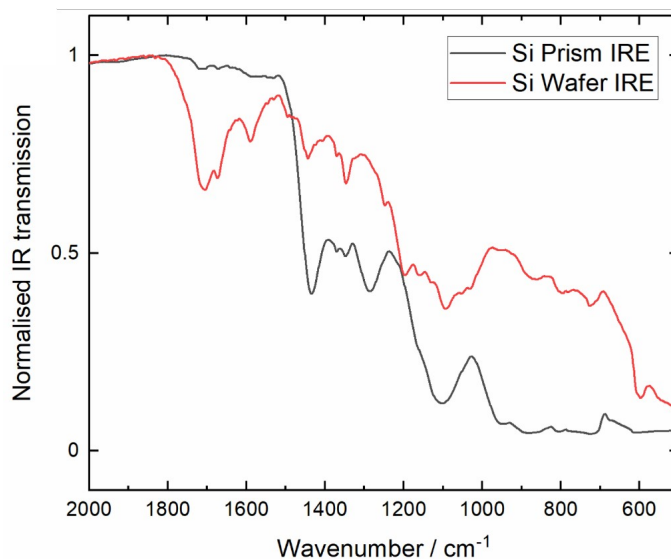


Figure 4. Normalised infrared transmission through the Si prism (black trace) and the Si wafer (red trace) internal reflection elements with a 20 nm Au layer within the assembled SEIRAS cell containing $[\text{Pyrr}_{13}][\text{TFSI}]$ electrolyte within an Ar atmosphere.



Electrochemical Characterisation

View Article Online

DOI: 10.1039/D5FD00174A

Cyclic voltammetry (CV) of a Au disk electrode (polycrystalline bulk Au, non-thin layer) in [Pyrr₁₃][TFSI] within a flooded three electrode cell shows a double layer region response between the potential ranges of -2.96 to +1.54 V vs. Fc⁺/Fc (**Figure 5**). Enlargement of the potential window beyond the oxidative and reductive potential limits between -3.46 to +2.55 V results in multiple broad cathodic and anodic peaks as reported previously,¹⁸ wherein reductive or oxidative decomposition results in the observation of additional peaks on the corresponding reverse sweep.⁶ The non-faradaic CV window was considered when setting potential limits with the SEIRAS cell using a pseudo Ag wire reference.

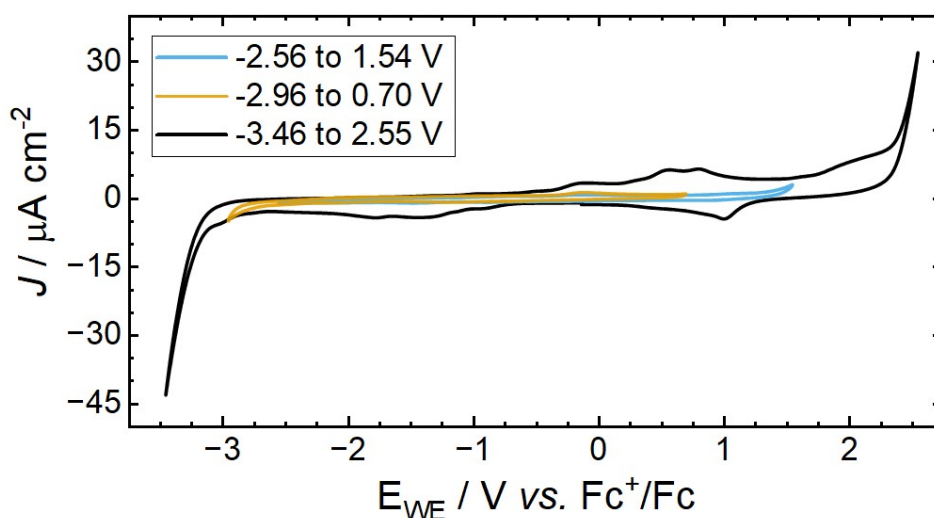


Figure 5. CVs of [Pyrr₁₃][TFSI] at a Au disk electrode at 100 mV s⁻¹ within different potential windows, measured at 23°C under Ar.

Effect of the addition of Li⁺ on cation-anion organisation

For Li-O₂ or Li-ion cells, Li⁺ also needs to be present in the electrolyte to take part in the reactions that occur at the interface. Understanding the structure of the Au/IL interface in the presence of metal cations closer represents model battery electrolyte systems. To determine the impact of Li⁺ ions on the potential-induced restructuring of the IL, cation/anion interfacial



restructuring was investigated in [Pyrr₁₃][TFSI] containing 0 mM, 1 mM and 100 mM Li[TFSI] and the CV is shown in **Figure 6a**. The CVs of 0 mM, 1 mM and 100 mM Li[TFSI] are all slightly different with numerous minor faradaic peaks appearing in the scan at varying potentials attributed to minor absorption events of IL constituent ions and trace impurities in the electrolyte or from the deposited Au surface.

View Article Online

DOI: 10.1039/D5FD00174A

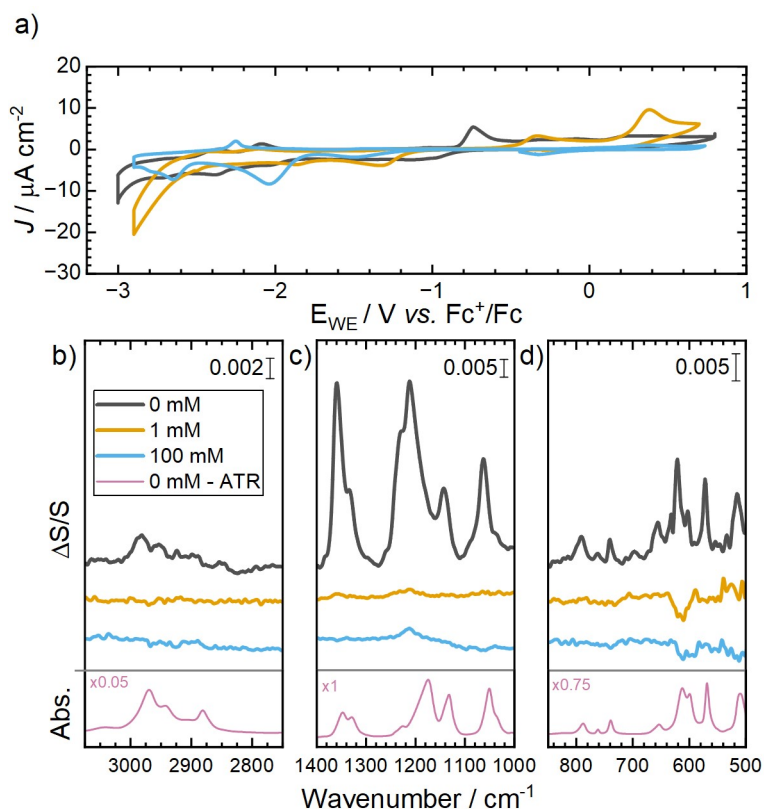


Figure 6. Potential-Induced Interfacial Restructuring of IL + Li⁺ solutions: (a) Cyclic voltammogram (2 mV s⁻¹ scan rate) of a 20 nm Au layer on a Si wafer with 0, 1 and 100 mM Li[TFSI]/[Pyrr₁₃][TFSI] electrolyte. (b-d) *In situ* ATR-SEIRAS spectra of a 20 nm Au layer on a Si wafer with 0, 1, and 100 mM Li[TFSI] in [Pyrr₁₃][TFSI] electrolyte taken at +0.7 V vs. Fc⁺/Fc at (b) 3080-2780 cm⁻¹, (c) 1400-1000 cm⁻¹, and (d) 1000-500 cm⁻¹. The bottom spectra in (b-d) are diamond-ATR spectra of the neat IL (0 mM), where the multiplication factors show the relative absorbance intensities of the different spectral regions relative to the central panel. SEIRA spectra are shown in **Figure 6 b-d** compare all Li-salt concentrations in the IL electrolyte at 0.7 V (where the reference spectrum was collected at the negative vertex



potential). Within the neat IL electrolyte (0 mM), the SEIRA spectrum shows the formation of large positive peaks ascribed to the [TFSI]⁻ anion (spanning *ca.* 1400-1000 cm⁻¹) accumulating

View Article Online

DOI: 10.1039/D5FD00174A

in the interfacial region as the surface charge of the Au becomes more positive. The full band assignments are provided in **Table 1** and the majority of IL bands show almost directly equivalent bands/shapes in conventional diamond-ATR spectrum (*i.e.*, no Au layer) of the neat [Pyr₁₁][TFSI] IL (0 mM) shown at the bottom Figure 6 b-d (plotted within an independent absorbance scale). The SEIRA effect is confined close to the Au surface and decreases rapidly, meaning the observed bands arise primarily from changes in the first ionic layer and only some overlayers. However, while ion adsorption interactions at the Au/IL interface may effect specific band positions, the more significant differences in the intense C-F stretching modes (1231-1173 cm⁻¹) have also been ascribed to the significant dispersion of refractive index across this spectral region where these vibrational bands are most intense.³⁰ These differences have been observed previously with analogous [TFSI]⁻ containing ILs.^{14, 15, 18}

Within the main SEIRAS spectrum of the neat IL, the large changes in main bands following polarisation from negative to positive potentials align with previous observations of Motobayashi et al.,¹⁸ who investigated these neat IL systems in great depth, demonstrating the alkyllpyrrolidinium cations with [TFSI]⁻ anions induce larger asymmetric activation energy barriers (relative to comparative imidazolium systems) to drive double layer restructuring.^{14, 15} The voltage range applied here extends beyond required energy barriers to induce full cation-to-anion exchange at the interface. However, owing to the transmission properties of the Si microgroove wafer, vibrations below 1000 cm⁻¹ are also observed. Therein, bands below 1000 cm⁻¹ relating to the [TFSI]⁻ anion vibrations were also found to grow positively during this potential range, correlating with anion-related bands at higher wavenumbers, demonstrating the value in the wafer compared to conventional Si IREs.



Table 1. Peak positions and assignments for the peaks in **Figure 6** from the Si wafer ATR-SEIRA and diamond-ATR-FTIR spectra of Ar-purged [Pyrr₁₃][TFSI]. Literature values from

View Article Online
DOI: 10.1039/D5FD00174A

18, 31-34

IL ion	Assignment	SEIRAS experimental / cm ⁻¹	ATR-FTIR experimental / cm ⁻¹	Literature / cm ⁻¹
[Pyrr ₁₃] ⁺	v _{as} (CH ₃) _{methyl}		3044	3028 ¹⁸
[Pyrr ₁₃] ⁺	v _{as} (CH ₃) _{alkyl}	2968	2970	2970 ¹⁸
[Pyrr ₁₃] ⁺	v _s (CH ₂) _{pyr}	2936	2942	2944 ¹⁸
[Pyrr ₁₃] ⁺	n _s (CH ₂) _{alkyl}	2908	2909	2907 ¹⁸
[Pyrr ₁₃] ⁺	n _s (CH ₂) _{alkyl}	2875	2881	2885 ¹⁸
[Pyrr ₁₃] ⁺	Ring mode	943	930	939 ³¹
[TFSI] ⁻	v _{as} (SO ₂) _{i.p.}	1359	1349	1362 ¹⁸
[TFSI] ⁻	n _{as} (SO ₂) _{o.p.}	1335	1330	1350 ¹⁸
[TFSI] ⁻	n _s (CF ₃)	1231	1223	1234 ¹⁸
[TFSI] ⁻	n _{as} (CF ₃)	1210	1173	1219 ¹⁸
[TFSI] ⁻	n _s (SO ₂)	1142	1131	1138 ¹⁸
[TFSI] ⁻	n _s (SNS)	1060	1060	1062 ¹⁸
[TFSI] ⁻	n _s (CS)	791	790	790 ^{31, 32}
[TFSI] ⁻	n _s (SNS)	763	763	762 ³²
[TFSI] ⁻	d _s (CF ₃)	740	740	740 ³¹⁻³⁴
[TFSI] ⁻	d(SNS)	657	655	655 ^{31, 32}
[TFSI] ⁻	δ _{as} (SO ₂)	621	614	618 ^{31, 32}
-	unassigned	600	600	-
[TFSI] ⁻	δ _{as} (CF ₃), n(CN)	571	570	574 ³¹
[TFSI] ⁻	δ _{as} (CF ₃)	515	511	514 ^{31, 32}

Upon addition of even minor concentrations of the Li[TFSI] salt in the IL, the resulting changes in the collected ATR-SEIRA spectra indicate a significant disruption in the layering of cation and anion in the IL. In both IL/Li-salt solutions, positive-going peaks resulting from the anion



are observed, though these are much less intense than those observed with pure IL, which demonstrates the disruption of ordering caused by the presence of Li^+ . This disruption of the highly ordered double layer structuring occurs even at very low concentrations of Li salt, where at 1 mM $\text{Li}[\text{TFSI}]$ in $[\text{Pyrr13}][\text{TFSI}]$ the significant growth in the main bands associated with $[\text{TFSI}]^-$ anions at the surface is not observed.

View Article Online

DOI: 10.1039/D5FD00174A

Changes within Raman spectra of the IL/Li-salt solutions (**Figure 7**) can be used to derive information on the coordination environment of the $[\text{TFSI}]^-$ anion, informing on the formation of complexes that would be present in the bulk solution and at/near electrode interfaces. The changes in the Raman vibrational mode of $[\text{TFSI}]^-$ at *ca.* $740\text{-}742\text{ cm}^{-1}$ as lithium is introduced into the IL can be used to inform on coordination between $[\text{TFSI}]^-$ with the dissolved Li^+ cation.^{17, 35, 36} As Li^+ increases, the formation of a second band at *ca.* 748 cm^{-1} is ascribed to the $[\text{TFSI}]^-$ anion coordinating to Li^+ . From the ratios between the two overlapping modes (using the integrated intensities (I) of the normalised, deconvoluted bands), the proportion of coordinated (I_b) versus uncoordinated (I_f) $[\text{TFSI}]^-$ species can be estimated (shown as % in **Figure 7**). These results show roughly 5 and 10% of the anion in solution is involved in some form of coordination interaction for the 1 and 100 mM solutions, respectively.



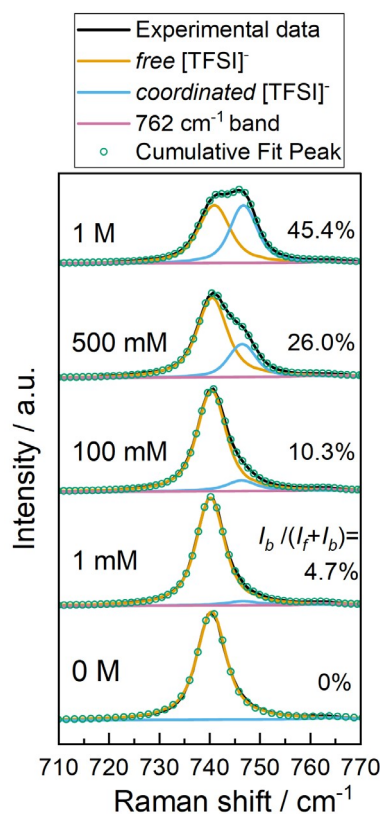


Figure 7. Raman spectra of bulk IL/IL-salt solutions collected using 785 nm laser excitation. Bands were deconvoluted into two primary peaks ascribed the *free* and *coordinated* [TFSI]⁻ and the values show the percentages of *coordinated* [TFSI]⁻ in solutions. A minor band at 762 cm⁻¹ (n_s(SNS)) is included in all fitted data sets.

In these IL solutions, the Li⁺ cation behaves unlike the bulky organic pyrrolidinium cation, coordinating reasonably strongly with [TFSI]⁻, leading to larger complexes such as [Li[TFSI]₂]⁻ or [Li[TFSI]₃]²⁻ at low to intermediate concentrations. At higher concentrations, Li[TFSI]₁ ion pairs may become favoured, and agglomerations/aggregations are possible. For low concentrations, these larger complexes that form only in minor amounts appear to change the distribution of ionic species sufficiently to significantly alter double layer structuring. Therein, [Li[TFSI]_x]^{(x-1)-} species are less likely to be treated as point charges that can readily arrange at the electrode surface to give ‘well defined’ periodic double layers. It would be valuable to

investigate more dilute solutions (<1 mM Li[TFSI]) by ATR-SEIRAS where the proportion of large complexes is reduced to fully identify the role of small metal cations in disrupting the organisation of IL double layers. However, such low concentrations have limited practical value for battery electrolytes and were beyond the scope of this work.

View Article Online
DOI: 10.1039/D5FD00174A

Effect of the addition of electrochemically active dissolved O₂ on the cation-anion double layer organisation

ILs are an interesting class of materials for electrolytes for Li-O₂ battery chemistries, especially due to the negligible volatility of ILs that would be valuable to mitigate evaporation issues within systems that could be operated under *open* or dynamic gas flow conditions. Therein, a key aspect of the reaction at the positive electrode in Li-O₂ cells is the reduction of O₂, leading to the formation of Li₂O₂ as a final discharge product most commonly. As such, the effect of dissolved O₂ as a redox active solute on the behaviour and structuring of the IL electrolyte at the interface, without any dissolved Li-salt, was studied using ATR-SEIRAS.

For Li-O₂ positive electrodes, O₂ reduction occurs at more positive regions than reported in previous figures. Thus, the behaviour of the IL with and without O₂ was studied within a reduced potential window of -1.7 V to 0 V vs. Fc⁺/Fc using the equivalent thin Au layer working electrode in the ATR-SEIRAS spectroelectrochemical cell. The CV collected under Ar in this window shows a double layer region with no Faradaic peaks (**Figure 8a**). On addition of dissolved O₂, and cycled within the same potential range, a quasi-reversible redox process is observed centred at *ca.* -1.3 V vs. Fc⁺/Fc, attributed to the 1e⁻ O₂/O₂⁻ redox couple.³⁷⁻³⁹



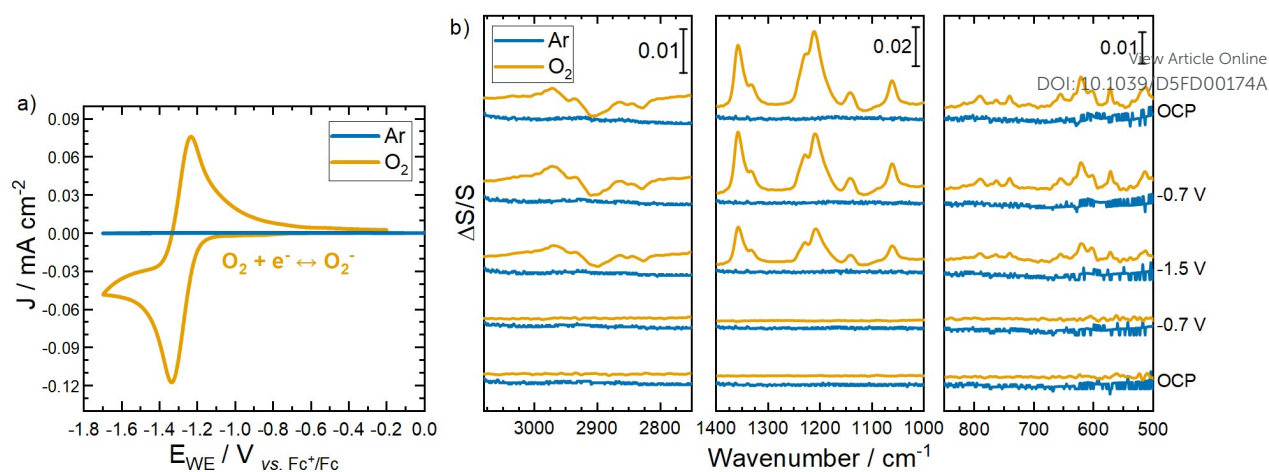


Figure 8. (a) Cyclic voltammogram and (b) *in situ* ATR-SERIA spectra of $[\text{Pyrr}_{13}][\text{TFSI}]$ electrolyte at a 20 nm Au layer on Si wafer under Ar (blue traces) and O_2 (red traces).

The SEIRA spectra of $[\text{Pyrr}_{13}][\text{TFSI}]$ collected under Ar in this reduced potential window range of -1.7 V to 0 V shows no significant peak changes and the baseline remains fairly flat under all potentials (**Figure 8b**). This potential range is too narrow to overcome the required energy barriers to trigger any detectable initial organisation of the double layer. As such, without driving the electrode to sufficiently low potentials to promote the formation of a structured, periodic double layer, no such organisation or reorganisation is observed on cycling.

However, after addition of dissolved O_2 into the electrolyte, the reduction of O_2 at the Au electrode coincides with significant changes observed in the collected SEIRA spectra in **Figure 8b**. From the onset of the oxygen reduction reaction (ORR), a growth in the intensity of $[\text{TFSI}]^-$ anion related bands are observed in mid and low wavenumber regions, coinciding with negative-going peaks from the CH stretches of the cation in the high wavenumber region from $[\text{Pyrr}_{13}]^+$. These results initially demonstrate the redox couple involving the formation of the superoxide radical strongly affects double layer properties of the IL. Positive going $[\text{TFSI}]^-$ peaks indicate greater proportion of the anion arriving at the surface as the reaction progresses, with reduction of the cation species (confirmed by growth of negative peaks in high

wavenumber regions). While this data may not confirm the formation of, or complete restructuring of, the double layer periodicity discussed previously, it may reasonably show that the oxygen redox drives a change in the interface state from organised to disorganised (or vice versa). Within these IL electrolytes, weak stabilisation interactions would be expected between the superoxide O_2^- radical anions and the $[Pyrr_{13}]^+$ cations.^{40, 41} These weak interactions, coinciding with growing diffusion gradients as the reaction proceeds, appear to disrupt the IL layers close to the surface, promoting more facile cation-to-anion replacement at the surface.

The relative abundance of the anion at the surface increases throughout the ORR/OER (oxygen evolution reaction), such that even as the sweep direction is reversed and the re-oxidation of the dissolved superoxide becomes the dominant process, the positive $[TFSI]^-$ peaks (and negative $[Pyrr_{13}]^+$ peaks) appear to grow continually. While it is not expected for the interfacial (dis)organisation to fully revert to its initial reference state after the electrochemical reaction is finished, the differences between the initial and final spectra after one full cycle are notable considering the general chemical reversibility of the ORR/OER redox couple in these systems.

To quantify these changes, the evolution of SEIRA spectra during ORR/OER is shown in **Figure 9a** and the integrated band intensities of the $\nu_{as}(SO_2)_{i.p.}$ and $\nu_{as}(CF_3)$ peaks as a function of potential are shown in **Figure 9b**. As the potential is scanned negatively, initially these bands relating to the $[TFSI]^-$ anion appear as very small negative-going bands, until -1.06 V, when the bands become positive-going and continue to increase in intensity as the potential is scanned to -1.7 V and back up to 0.2 V. The initial loss of $[TFSI]^-$ at the interface is unsurprising as it is expected that the anions move away from the interface as the surface becomes more negative. The $[TFSI]^-$ bands begin to grow positively at -1.06 V which is the onset potential for the ORR, as shown in the CV in **Figure 8a**. The changes observed in the SEIRA spectra are, thereby, caused by the generation of superoxide (O_2^-) at the electrode surface. It is likely that the



generation of a negative superoxide ion that is weakly associated with $[\text{Pyrr}_{13}]^+$ significantly disrupts the ordering of the IL anions in particular local to the interface, perhaps also disrupting weak associations between $[\text{TFSI}]^-$ anions and $[\text{Pyrr}_{13}]^+$ cations. $[\text{TFSI}]^-$ may reorientate at the interface to compensate for this change. Additionally, the flux of dissolved O_2 and superoxide (to and from the IL/electrode interface) will have an influence in perturbing the interfacial region in general.

View Article Online

DOI: 10.1039/D5FD00174A

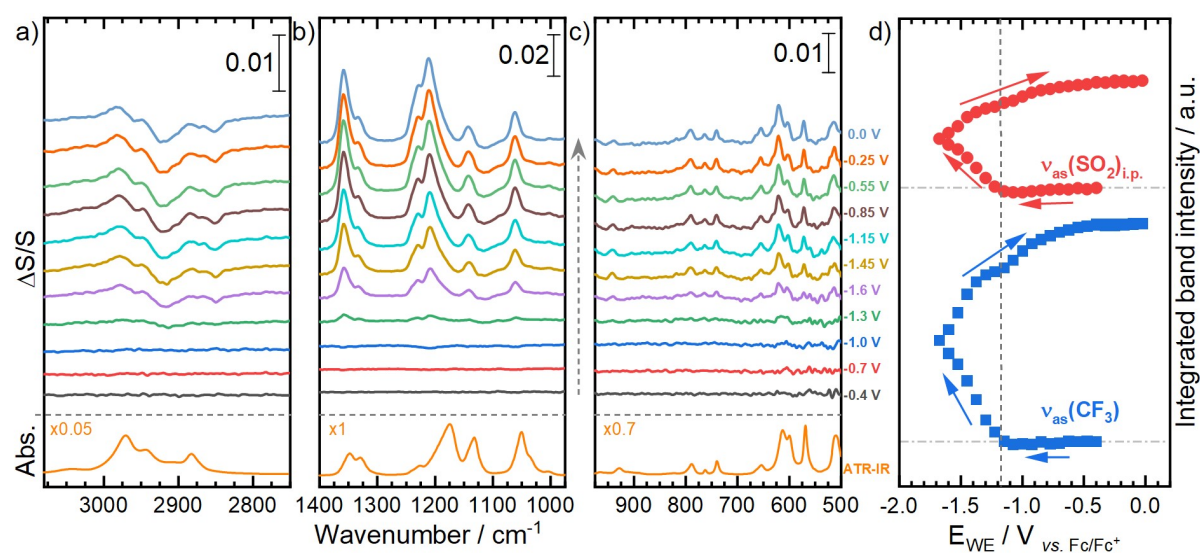


Figure 9. Evolution of (a) ATR-SEIRA spectra during cyclic voltammetry of O_2 -saturated $[\text{Pyrr}_{13}][\text{TFSI}]$ electrolyte at a 20 nm Au layer on Si wafer and (b) the integral intensities of primary peaks ascribed to the $[\text{TFSI}]^-$ anion ($\nu_{\text{as}}(\text{CF}_3)$ at 1209 cm^{-1} and $\nu_{\text{as}}(\text{SO}_2)_{\text{i.p.}}$ at 1357 cm^{-1}). Integral intensities are shown stack plotted by peak group where the horizontal dash-dot lines show the zero-intensity line of each band from the initial reference spectrum.

Even upon reversal of the potential sweep direction to drive the OER and to even higher potentials, the intensity of these positive-going $[\text{TFSI}]^-$ peaks increases further (**Figure 9b**). These changes are matched with continual growth of the low wavenumber peaks that are



observable with the microgroove Si wafer, and the growth of negative going peaks arising from depletion of the cation at the interface. Only after the cell voltage is increased above *ca.* -0.5 V vs. Fc^+/Fc the peak intensities appear to plateau, indicating no further potential-induced restructuring, but the changes induced in the interface structure are not at all reversed as the electrode potential is returned to initial values.

View Article Online

DOI: 10.1039/D5FD00174A



Conclusions

Cation-anion restructuring of 1-methyl-1-propylpyrrolidinium bis ((trifluoromethyl)sulfonyl)imide ([Pyrr₁₃][TFSI]) with and without the presence of Li⁺ and O₂ at an electrified Au/IL interface was investigated under potential control using *in situ* electrochemical attenuated total reflection surface-enhanced infrared absorption spectroscopy (ATR-SEIRAS). The use of a micromachined Si wafers and a custom spectroelectrochemical cell enabled SEIRA spectra to be collected down to 500 cm⁻¹ within a non-aqueous IL electrolyte under well controlled atmospheres. The spectra enabled a good signal/noise ratio and allowed the detection of newly observed potential dependent bands below 1000 cm⁻¹ relating primarily to the accumulation of [TFSI]⁻ anions at the surface correlating with changes in higher wavenumber regions. The double layer restructuring observed within this neat IL was significantly disrupted with the addition of low concentrations (0.001 M) of Li-salt. The addition of the Li⁺ cation resulted in the formation of [Li[TFSI]_x]^{-(x-1)} complexes and aggregates which disrupted the behaviour and periodicity of the double layer compared to the neat IL. Inclusion of redox-active dissolved dioxygen into the IL enabled the reduction of O₂ to reversibly form superoxide (O₂⁻), promoting irreversible double layer rearrangement within a narrower electrode potential window. Therein, weak coordination between the superoxide product and the IL cation (O₂⁻ ---[Pyrr₁₃]⁺), and its impact on interactions between IL cations and anions, disrupts double layer structuring and reduced energy barriers for accumulation of [TFSI]⁻ at the surface.



AUTHOR CONTRIBUTIONS

View Article Online
DOI: 10.1039/D5FD00174A

L.J.W. performed the SEIRAS experiments and analysed the data. T.S. performed the electrochemical characterisation. K.C. carried out supporting electrochemical and spectroscopic measurements, A.R.N. supported methodology development and data analysis. L.J.H. and R.N. provided supervision, resources, and project administration. All authors discussed the results and contributed to writing – review and editing.

ACKNOWLEDGEMENTS

The authors acknowledge Rory Powell for carrying out the SEM and David Costa Milan for AFM images of the evaporated gold layer. L.J.W. acknowledges PhD funding support from the UKRI (EPSRC DTP). L.J.H, and A.R.N acknowledge the financial support from the Faraday Institution CATMAT (EP/S003053/1, FIRG016).

CONFLICTS OF INTEREST

There are no conflicts to declare



References

1. M. Armand, F. Endres, D. R. MacFarlane, H. Ohno and B. Scrosati, *Nat. Mater.*, 2009, **8**, 621-629.
2. M. C. Buzzeo, R. G. Evans and R. G. Compton, *ChemPhysChem*, 2004, **5**, 1106-1120.
3. M. Galiński, A. Lewandowski and I. Stepniak, *Electrochim. Acta*, 2006, **51**, 5567-5580.
4. D. R. MacFarlane, N. Tachikawa, M. Forsyth, J. M. Pringle, P. C. Howlett, G. D. Elliott, J. H. Davis, M. Watanabe, P. Simon and C. A. Angell, *Energy Environ. Sci.*, 2014, **7**, 232-250.
5. X. Tang, S. Lv, K. Jiang, G. Zhou and X. Liu, *J. Power Sources*, 2022, **542**, 231792.
6. A. R. Neale, S. Murphy, P. Goodrich, C. Hardacre and J. Jacquemin, *ChemPhysChem*, 2017, **18**, 2040-2057.
7. S. Baldelli, *Acc. Chem. Res.*, 2008, **41**, 421-431.
8. S. Rivera-Rubero and S. Baldelli, *J. Phys. Chem. B*, 2004, **108**, 15133-15140.
9. C. Aliaga and S. Baldelli, *J. Phys. Chem. B*, 2006, **110**, 18481-18491.
10. N. Nanbu, T. Kato, Y. Sasaki and F. Kitamura, *Electrochemistry*, 2005, **73**, 610-613.
11. N. Nanbu, Y. Sasaki and F. Kitamura, *Electrochem. Commun.*, 2003, **5**, 383-387.
12. V. O. Santos, M. B. Alves, M. S. Carvalho, P. A. Z. Suarez and J. C. Rubim, *J. Phys. Chem. B*, 2006, **110**, 20379-20385.
13. Y.-X. Yuan, T.-C. Niu, M.-M. Xu, J.-L. Yao and R.-A. Gu, *J. Raman Spectrosc.*, 2010, **41**, 516-523.
14. K. Motobayashi, K. Minami, N. Nishi, T. Sakka and M. Osawa, *J. Phys. Chem. Lett.*, 2013, **4**, 3110-3114.
15. K. Motobayashi, N. Nishi, Y. Inoue, K. Minami, T. Sakka and M. Osawa, *J. Electroanal. Chem.*, 2017, **800**, 126-133.
16. G. A. Elia, J. Hassoun, W. J. Kwak, Y. K. Sun, B. Scrosati, F. Mueller, D. Bresser, S. Passerini, P. Oberhumer, N. Tsiouvaras and J. Reiter, *Nano Lett.*, 2014, **14**, 6572-6577.



17. A. R. Neale, R. Sharpe, S. R. Yeandel, C.-H. Yen, K. V. Luzyanin, P. Goddard, E. A. Petrucco and L. J. Hardwick, *Adv. Funct. Mater.*, 2021, **31**, 2010627. View Article Online
DOI: 10.1039/D5FD00174A
18. K. Motobayashi, Y. Shibamura and K. Ikeda, *Electrochem. Commun.*, 2019, **100**, 117-120.
19. K. T. Queeney, H. Fukidome, E. E. Chaban and Y. J. Chabal, *J. Phys. Chem. B*, 2001, **105**, 3903-3907.
20. R. Herzig-Marx, K. T. Queeney, R. J. Jackman, M. A. Schmidt and K. F. Jensen, *Anal. Chem.*, 2004, **76**, 6476-6483.
21. E. Karabudak, B. L. Mojet, S. Schlautmann, G. Mul and H. J. G. E. Gardeniers, *Anal. Chem.*, 2012, **84**, 3132-3137.
22. E. Karabudak, *Electrophoresis*, 2014, **35**, 236-244.
23. M.-h. Shao, P. Liu and R. R. Adzic, *J. Am. Chem. Soc.*, 2006, **128**, 7408-7409.
24. X.-K. Xue, J.-Y. Wang, Q.-X. Li, Yan, J.-H. Liu and W.-B. Cai, *Anal. Chem.*, 2008, **80**, 166-171.
25. H. Schumacher, U. Künzelmann, B. Vasilev, K.-J. Eichhorn and J. W. Bartha, *Appl. Spectrosc.*, 2010, **64**, 1022-1027.
26. T. A. Morhart, B. Unni, M. J. Lardner and I. J. Burgess, *Anal. Chem.*, 2017, **89**, 11818-11824.
27. G. A. Snook, A. S. Best, A. G. Pandolfo and A. F. Hollenkamp, *Electrochem. Commun.*, 2006, **8**, 1405-1411.
28. J. P. Vivek, N. Berry, G. Papageorgiou, R. J. Nichols and L. J. Hardwick, *J. Am. Chem. Soc.*, 2016, **138**, 3745-3751.
29. J. P. Vivek, N. G. Berry, J. Zou, R. J. Nichols and L. J. Hardwick, *J. Phys. Chem. C*, 2017, **121**, 19657-19667.
30. T. Buffeteau, J. Grondin and J.-C. Lassègues, *Appl. Spectrosc.*, 2010, **64**, 112-119.



31. P. C. Howlett, N. Brack, A. F. Hollenkamp, M. Forsyth and D. R. MacFarlane, *J. Electrochem. Soc.*, 2006, **153**, A595.
32. I. Rey, P. Johansson, J. Lindgren, J. C. Lassègues, J. Grondin and L. Servant, *J. Phys. Chem. A*, 1998, **102**, 3249-3258.
33. I. Rey, J. L. Bruneel, J. Grondin, L. Servant and J. C. Lassègues, *J. Electrochem. Soc.*, 1998, **145**, 3034.
34. Z. Wang, W. Gao, X. Huang, Y. Mo and L. Chen, *J. Raman Spectrosc.*, 2001, **32**, 900-905.
35. M. Kunze, E. Paillard, S. Jeong, G. B. Appetecchi, M. Schönhoff, M. Winter and S. Passerini, *J. Phys. Chem. C*, 2011, **115**, 19431-19436.
36. M. Castriota, T. Caruso, R. G. Agostino, E. Cazzanelli, W. A. Henderson and S. Passerini, *J. Phys. Chem. A*, 2005, **109**, 92-96.
37. A. W. Lodge, M. J. Lacey, M. Fitt, N. Garcia-Araez and J. R. Owen, *Electrochim. Acta*, 2014, **140**, 168-173.
38. S. Monaco, A. M. Arangio, F. Soavi, M. Mastragostino, E. Paillard and S. Passerini, *Electrochim. Acta*, 2012, **83**, 94-104.
39. A. R. Neale, P. Goodrich, T.-L. Hughes, C. Hardacre, S. C. Ball and J. Jacquemin, *J. Electrochem. Soc.*, 2017, **164**, H5124-H5134.
40. P. M. Radjenovic and L. J. Hardwick, *Faraday Discuss.*, 2018, **206**, 379-392.
41. P. M. Radjenovic and L. J. Hardwick, *Phys. Chem. Chem. Phys.*, 2019, **21**, 1552-1563.

View Article Online
DOI: 10.1039/D5FD00174A

